Research Square

Preprints are preliminary reports that have not undergone peer review.
They should not be considered conclusive, used to inform clinical practice,
or referenced by the media as validated information.

Preparation and characterization of biodegradable films based on chitosan/poly(vinyl alcohol) incorporating selenium-immobilized graphene oxide for fruit preservation

Nguyen Ngoc Kim Tuyen
Ho Chi Minh City University of Industry and Trade
Nguyen Minh Dat
Ho Chi Minh City University of Technology
Tran Do Dat
Ho Chi Minh City University of Technology
Nguyen Huu Hieu
nhhieubk@hcmut.edu.vn

Ho Chi Minh City University of Technology

Research Article

Keywords: Chitosan, poly(vinyl alcohol), selenium, graphene oxide, food preservation

Posted Date: March 13th, 2026

DOI: https://doi.org/10.21203/rs.3.rs-9065787/v1

License: This work is licensed under a Creative Commons Attribution 4.0 International License.
Read Full License

Additional Declarations: No competing interests reported.

Version of Record: A version of this preprint was published at Chemical Papers on May 25th, 2026. See the published version at https://doi.org/10.1007/s11696-026-05051-6.

Preparation and characterization of biodegradable films based on chitosan/poly(vinyl alcohol) incorporating selenium-immobilized graphene oxide for fruit preservation

Nguyen Ngoc Kim Tuyen[1,2,3,4], Nguyen Minh Dat[1,2,3],
Tran Do Dat[1,2,3], and Nguyen Huu Hieu[1,2,3*]

[1]*VNU-HCM, Key Laboratory of Chemical Engineering and Petroleum Processing (Key CEPP Lab), Ho Chi Minh City University of Technology (HCMUT), 268 Ly Thuong Kiet Street, Dien Hong Ward, Ho Chi Minh City, Vietnam*

[2]*Faculty of Chemical Engineering, Ho Chi Minh City University of Technology (HCMUT), 268 Ly Thuong Kiet Street, Dien Hong Ward, Ho Chi Minh City, Vietnam*

[3]*Vietnam National University Ho Chi Minh City (VNU-HCM), Linh Xuan Ward, Ho Chi Minh City, Vietnam*

[4]*Ho Chi Minh City University of Industry and Trade, 140 Le Trong Tan, Tan Phu District, Ho Chi Minh City, Vietnam*

**Corresponding author, email: nhhieubk@hcmut.edu.vn*

Abstract

Postharvest microbial contamination and moisture loss significantly shorten the shelf life of fresh produce, creating demand for biodegradable films with integrated antibacterial function. In this study, a three-component film composed of chitosan (CTS), poly(vinyl alcohol) (PVA), and graphene oxide-based selenium (SeGO) was fabricated via solution casting. Selenium microparticles were synthesized using *Psidium guajava* leaf extract and anchored onto graphene oxide sheets through ex situ ultrasonication. The combined effects of CTS, PVA, and SeGO on antibacterial activity against *Escherichia coli* were optimized using Response Surface Methodology based on a Box–Behnken design. The optimal ratio (CTS:PVA:SeGO = 2:4:2) achieved 99.99% inhibition, consistent with the predicted value ($p < 0.05$). Structural and physicochemical properties were characterized by FTIR, SEM-EDS, XRD, mechanical testing, swelling, and water vapor permeability analyses. The optimized film exhibited superior antibacterial performance compared with CTS, CTS-PVA, and CTS-SeGO films. In postharvest evaluation, *Manilkara zapota* coated with the optimized film showed reduced weight loss and no

fungal growth after 6 days of storage. These findings demonstrate the potential of CTS/PVA/SeGO films for sustainable food packaging applications.

Keywords: Chitosan, poly(vinyl alcohol), selenium, graphene oxide, food preservation.

1. Introduction

Chitosan (CTS), a copolymer of glucosamine and N-acetyl glucosamine units linked by 1-4 glycosidic bonds, is obtained by N-deacetylation of chitin, which is one of the most abundant natural amino polysaccharides [1]. CTS is a green polymer due to its dual characteristics of biodegradability and biocompatibility, enabling it to interact with biomolecules without causing their degradation [2]. Because of its biodegradability, CTS is utilized in the medical industry not just as a scaffold but also as a material for the manufacture of nanoparticles, which are used to administer numerous medications and vaccines *via* a variety of delivery methods. In addition, CTS is also applied to produce food preservation screens from microbial degradation. This is due to its excellent oxygen and carbon dioxide barrier properties and interesting antimicrobial properties. Nevertheless, the mechanical and waterproof qualities of chitosan-based films are readily impacted by pH and humidity conditions, which limits the packing application range. Associating chitosan with a moisture-resistant polymer while preserving the product's overall biodegradability is one way to get around this problem [3].

The physical and mechanical properties of the material are improved when cross-linked polymers like polyethylene terephthalate (PET) or polyurethane (PU) are combined with CTS. Tight bonding between polymer chains can be assisted by the cross-links, creating a network structure that optimizes tensile strength and hardness. Similarly, when CTS is combined with water-resistant polymers such as polyvinyl chloride (PVC), polypropylene (PP), and polyethylene (PE), it provides the ability to prevent water and liquid penetration. Moreover, an investigation has revealed that the amalgamation of collagen and gelatin results in higher mechanical and physical robustness, along with heightened biological activity. Gelatin is a biological material that is widely used in packaging technology because of its proline, glycine, and hydroxyproline contents [4]. However, combining CTS with cross-linked substances also has some disadvantages. Particularly, aggregation may reduce the aforementioned flux because the cross-linking agents tighten the network and limit the space between molecules, which decreases the gas molecules' freedom of movement across the film. Furthermore, combining crosslinking agents with CTS can lessen the elasticity and ductility of the film because they frequently possess hard, tensile, and inelastic

qualities. Various techniques for combining –CH with other polymers like poly(lactic-co-glycolic acid), polyethylene, etc. to create composites have been developed to promote the mechanical properties and degradation time [5]. Poly(vinyl alcohol) (PVA) is a synthetic water-soluble polymer with excellent film-forming properties, offering advantages such as good tensile strength, flexibility, and barrier properties to oxygen and aroma. PVA is an aliphatic polymer containing hydroxyl groups. It is widely used due to its non-toxicity, high water absorption capability, chemical resistance, biodegradability, and biocompatibility. Additionally, PVA exhibits favorable properties for the production of flexible films for food packaging and controlled drug delivery systems, including films and strips for localized application in the periodontal pocket [6 – 8].

Selenium microparticles (SeMPs), graphene oxide (GO), and graphene oxide-based selenium (SeGO) nanocomposite are materials that have garnered significant interest in various fields. SeGO nanocomposite is formed by incorporating SeMPs into GO, offering a hybrid material with unique characteristics and applications. These materials hold promise in fields like medicine, electronics, environmental science, and more, owing to their diverse properties and potential functionalities [9 – 11]. SeMPs, GO, and SeGO stand at the forefront of bioactive materials, showcasing immense potential across diverse biomedical applications. Their collective bioactive properties present a transformative landscape in healthcare. SeMPs, owing to their antioxidative prowess, exhibit remarkable potential in mitigating oxidative stress-related ailments by efficiently penetrating cells. Meanwhile, the unique surface characteristics of the GO enable it to serve as a versatile platform for drug delivery systems. When combined into SeGO, these materials synergize their properties, amplifying their impact in combating bacterial infections, aiding in biomedical imaging techniques, supporting tissue regeneration, and even augmenting cancer therapies through targeted and enhanced treatment modalities. Their multifaceted bioactive nature positions these nanomaterials as frontrunners in revolutionizing medical interventions, diagnostics, and therapies, promising a paradigm shift in the realm of healthcare advancements [12].

The blending between CTS and PVA improves the mechanical strength and thermal stability, keeping the intrinsic properties of transparency and swelling ability of CTS films [13]. To accommodate active packaging, the improvement of the biological activity of the film, along with improving the film's characteristics through the combination of polymers. Active packaging is a packaging system that possesses attributes beyond basic barrier properties, which are achieved by adding active ingredients in the packaging system and/or using actively functional polymers [14].

The combination of antimicrobial agents is necessary and increasingly gaining noteworthy exploration. SeGO is added as an antibacterial agent to form a three-component film that enhances the film's biological efficiency. Accordingly, the presence of functional groups, such as carboxyl, epoxy, hydroxyl, etc., allows GO to become functionalized and exhibit robust interactions with proteins, lipids, and nucleic acids, among other biomolecules. SeMPs tend to exhibit positive charges that interact strongly with negative charges on the cell wall, causing bacterial intracellular damage and ion absorption. Combining these two components not only helps enhance the biological activity of the material but also increases the stability prevents Se coagulation and helps increase the efficiency and effectiveness as well as the ability of particles to interact with each other.

On the one hand, using the response surface methodology (RSM) is one attempt to modify the plastic's composition for improved performance. Despite the promising potential of nanocomposites, the widespread application of selenium nanoparticles in food packaging is currently hindered by two major challenges. First, conventional synthesis protocols often rely on toxic chemical reductants (e.g., sodium borohydride), raising safety concerns for food contact materials. Second, the direct incorporation of inorganic nanofillers into organic polymer matrices frequently results in particle agglomeration, which detrimentally affects the film's mechanical integrity and barrier performance. Consequently, there is a critical need for a 'green-on-green' synthesis strategy, where plant extracts serve as dual reducing and stabilizing agents to immobilize nanoparticles onto a carrier platform (such as graphene oxide), ensuring both biosafety and uniform dispersion within the polymer matrix. The main aim of this study is the design and fabrication of a biodegradable composite based on chitosan and PVA with the addition of SeGO as the antimicrobial agent. Since antibacterial activity is one of the crucial parameters for assessing the characterization of the film, the fabrication process is created using Design-Expert software *via* RSM Box-Behnken design. CTS and SeGO are two components that are believed to be biologically active in application and PVA is mixed in during the manufacturing process to improve the tensile strength, elasticity, and water resistance of the film. This makes films more applicable in a variety of industries, including the healthcare, environmental, and industrial sectors. Box-Behnken design is a recommended RSM method for optimizing processes with three variables, utilizing fewer experimental units due to the absence of axial/star runs. It is suitable for three-variable optimization as it requires a small number of samples. Optimizing the antibacterial

properties of materials impacted by independent factors including CTS, PVA, and SeGO is the aim of the experiment.

In this study, SeMPs were synthesized using *Psidium guajava* (*P. guajava*) as a green reducing and stabilizing agent, while the decoration of SeMPs onto the surface of the GO sheets was carried out under ultrasonication. Additionally, the study delved into the antibacterial effectiveness of *Escherichia coli* (*E. coli*) of films consisting of CTS, PVA, and SeGO. This exploration involved examining the mass ratio of these three components using the response surface method by employing the Box-Behnken model. The identified optimal film configuration is denoted as CTS-PVA-SeGO film. The SeMPs, GO, SeGO, and CTS-PVA-SeGO film were analyzed via modern techniques such as Fourier transform infrared spectroscopy (FTIR), X-ray diffraction (XRD), scanning electron microscopy-energy dispersive X-ray Spectroscopy (SEM-EDS), mechanical properties (max load, elasticity modulus, max load stress, break elong, thickness, and break energy), swelling degree, and water vapor permeability. Additionally, the as-prepared CTS-PVA-SeGO film was further investigated for its antibacterial ability (against *E. coli* and *S. aureus* strains) and albumin protein protection as compared to CTS, CTS-PVA, and CTS-SeGO, which were applied to preserve *Manilkara zapota* (sapodilla, sapôchê or hồng xiêm in Vietnamese) by determining the remaining sapodilla weight and total soluble solid evaluation.

2. Experimental

2.1. Materials and chemicals

Firstly, *P. guajava* leaves were collected from Cu Chi District, Ho Chi Minh City, Vietnam. Sapodilla was bought at the supermarket in Tay Ninh Province, Vietnam. Photos of *P. guajava leaves* and sapodilla fruit are shown in the Figure 1. Chitosan powder was supplied from Shanghai Lanji Technology Development Co. Graphite (particle size < 20 μm, Gi), sodium selenite (Na_2SeO_3), and potassium bromide (KBr) were purchased from Sigma-Aldrich Co. Ltd, USA. Sulfuric acid (H_2SO_4), potassium permanganate ($KMnO_4$), poly(vinyl alcohol) (PVA), acetic acid (CH_3COOH), calcium chloride ($CaCl_2$), monopotassium phosphate (KH_2PO_4), disodium hydrogen phosphate ($Na\text{-}_2HPO_4$), sodium chloride (NaCl), and potassium chloride (KCl) were purchased from Xilong Scientific Co. Ltd, China. LB-Broth medium, LB-Agar, and egg albumin powder were purchased from HiMedia Laboratories Pvt. Ltd., India. Bacterial strains of *E. coli* ATCC® 25923™ and *S. aureus* ATCC® 25922™ were obtained from Ho Chi Minh City Pasteur Institute, Vietnam.

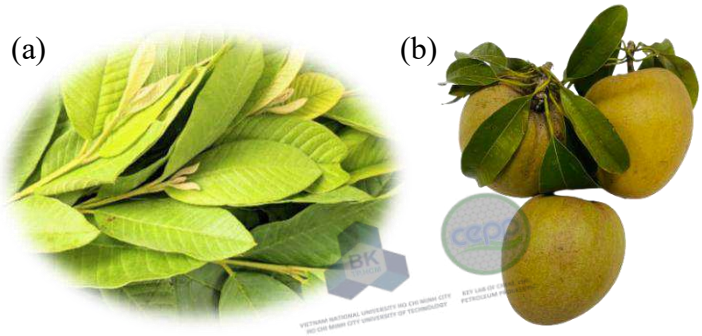


Figure 1. (a) *P. guajava* leaves and (b) sapodilla fruit

2.2. Preparation of *P. guajava* leaf extract

The *P. guajava* leaves were dried, finely ground, and preserved at room temperature. The powder was mixed with water at a concentration of 50 g/L and stirred at 90°C for 1 hour. Subsequently, the extracted solution was collected by removing leaf residue under vacuum filtration and was stored at 4°C.

2.3. Synthesis of SeMPs, GO, and SeGO

Accordingly, SeGO material was synthesized according to previously optimized research [15]. Firstly, SeMPs were synthesized through a green method utilizing the aqueous extract of *P. guajava* as a reducing agent and Na_2SeO_3 was employed as the precursor. The volumetric ratio between Na_2SeO_3 (5 g/L) and the extract was selected at 1:2. The mixture was stirred uniformly at 120°C for 90 minutes. After cooling, the color of the mixture turned to a red hue at room temperature. The resultant precipitate was obtained via centrifugation and subjected to drying at 70°C.

Second of all, GO was synthesized using an improved Hummers method [16]. A mixture of 400 mL of H_2SO_4 and H_3PO_4 (in a 9:1 ratio) was stirred at a temperature of 10°C after slowly adding 3 g Gi and 18 g $KMnO_4$. Once the mixture was well stirred, the temperature was raised to 50°C and stirred for 12 hours. After cooling the mixture temperature below 20°C, 500 mL of water was slowly added to the mixture. Hydrogen peroxide was employed until the mixture turned a bright yellow color. The resulting gel-like substance, obtained after centrifugation, was subjected to ultrasonic treatment for 24 hours for use in SeGO synthesis.

Finally, the SeGO material was synthesized using the *ex-situ* method. SeMPs and GO were mixed in a ratio of 1:2 and subjected to ultrasonic treatment for 24 hours. The obtained mixture was utilized in subsequent experiments.

177 **2.4. Preparation of CTS-PVA-SeGO film**

178 The film was fabricated from three different materials, including CTS, PVA, and SeGO. The
179 experimental design was constructed based on the Box-Behnken model with three varying factors,
180 which include the quantities of CTS, PVA, and SeGO. The range and levels of independent
181 variables including CTS, PVA, and SeGO content were coded with levels (−1, 0, 1), as
182 summarized in Table 1.

183 **Table 1.** Experimental variables for Box-Behnken statistical design

Factors	Unit	Abbreviations	Levels			Dependent variable
			−1	0	1	
CTS	g	C	1	2	3	
PVA	g	P	2	4	6	% inhibition
SeGO	mL	S	1	2	3	

184 Accordingly, the experiments comprised 17 runs with 3 factors, as shown in Table 2. Different
185 amounts of CTS (1, 2, and 3 g) were dissolved in 300 mL of 1% acetic acid by stirring and heating
186 at 80°C. Various amounts of PVA (2, 4, and 6 g) were dissolved in 300ml of water, stirred, and
187 heated at 80°C until completely dissolved. The two solutions were mixed in a 1:1 ratio (CTS:PVA).
188 Different volumes of SeGO (1, 2, and 3 mL) were added to the mixture, and the total volume was
189 adjusted to 60 mL. The mixture was stirred and sonicated to promote dispersion and remove
190 trapped gas bubbles before being poured into a Petri dish and dried at 40°C for 4 days.

191 The antibacterial activity of the film was evaluated with the percentage of inhibition against *E.*
192 *coli* as a target. 0.2 mL of the bacterial suspension from the experimental strain was cultured and
193 adjusted to a uniform concentration in test tubes containing Luria-Bertani broth (LB-broth)
194 medium. 0.2 mL of the film solution was added to the test tubes containing bacteria and bacterial
195 growth was allowed for 20 hours. The samples without the film solution and without bacterial
196 supernatant were considered the negative control and extraction controls, respectively. Bacterial
197 density was determined using the spectrophotometric absorbance method at a wavelength of 600
198 nm. The percentage of bacterial inhibition of the material was calculated using the following
199 Equation (1):

$$\%\ \text{inhibiton} = \frac{\text{Ac} - \text{At}}{\text{Ac}} \times 100\% \quad (1)$$

where Ac is the absorbance of the negative control sample and At is the absorbance of the test sample. The empirical data were analyzed by Design Expert® (11.0, Stat-Ease Inc., USA) software. The analysis of variance (ANOVA) was calculated from the factor of regression equation by empirical data and the proposal of an ideal condition for the model.

2.5. Characterization of materials and films

2.5.1. Characterization of SeMPs, GO, and SeGO

The materials were characterized using advanced analytical techniques. Specifically, FTIR conducted with an Alpha-E spectrometer from Bruker Optik GmbH, located in Ettlingen, Germany, was employed. This technique enabled the categorization of functional groups present on the surface of the GO, SeMPs, and SeGO by compressing the sample with KBr and analyzing the wavelength range from 4000 to 600 cm^{-1}. The SEM-EDS (Jeol-JMS 6490, Japan) was also used to investigate the composition of elements C, O, Se, and other elements in SeGO.

2.5.2. Characterization of film

In turn, the FTIR and SEM-EDX analyses of the film were conducted similarly to the procedure of the materials. Additionally, the D2 Phaser, manufactured by Brucker in Germany, was employed for XRD (X-ray Diffraction) analysis of the films. This analysis utilized CuKα radiation with a wavelength (λ) of 0.154 nm, exploring a range spanning from 5 to 80° to assess the structural properties and crystallinity of the films. For the characteristics of the film, the processes were described as follows:

a) Mechanical properties

The thickness, tensile strength, and elongation at the breakpoint of the films underwent testing following methods akin to those outlined [20]. All films, sized at 2×8 cm, were assessed utilizing a texture analyzer (AG-Xplus Series Precision Universal Testers). To ensure accuracy, each film underwent measurements at least four times to gather averaged data.

b) Swelling property

The swelling degree of each film was assessed following the methodology [18]. Initially, each film, sized at 1×1 cm^2, was dried and weighed (m_0). Subsequently, these dried samples were immersed in a pH 7 solution for 24 hours. After removal from the solution, excess liquid was

blotted using filter paper, and the immediate weight (m_t) was measured. The swelling degree was determined using Equation (2):

$$\text{Swelling degree (\%)} = \frac{m_t}{m_0} \times 100\ (\%) \quad (2)$$

c) Water vapor permeability

The water vapor permeability (WVP) of each film was determined gravimetrically utilizing the wet cup method [17]. The films were sealed onto a test vessel, which measured 11.5 cm in depth and 2.8 cm in internal diameter, containing 5 g of thoroughly dried $CaCl_2$. Subsequently, the sealed test vessel was placed within a desiccator holding distilled water at a consistent temperature of 30°C. The weight of the test vessel was recorded at regular intervals of 24 hours over a span of 7 days. The calculation for WVP was derived using Equation (3):

$$WVP = \frac{M \times A}{t \times S \times \Delta P} \quad (3)$$

where M (g) represents the increased weight of the test vessel due to water vapor transmission, A (m) signifies the film thickness, t (s) denotes the time taken for the weight increase to occur, S (m^2) is the film permeation area, and ΔP refers to the partial water vapor pressure difference across the film, set at 4240 Pa at 30°C.

2.6. Bioactivities

2.6.1. Antibacterial activity

The disk diffusion method was employed to assess the antibacterial activity of the films. Background films were also used to evaluate their antibacterial properties. Accordingly, 100 µL of CTS, PVA, CTS-PVA, CTS-SeGO, and CTS-PVA-SeGO film solutions were pipetted into wells on NA agar plates containing bacteria. The diameter of the antibacterial zone was measured after 24 hours [21].

2.6.2. Anti-inflammatory activity

Film protein protection was investigated based on the decomposition of albumin under the effect of temperature. Specifically, 0.2 mL albumin 1% was incubated with 2 mL of material at different concentrations. The mixture was diluted to 5 mL using PBS (pH 7). The reaction was incubated at room temperature for 30 minutes and heat-shocked at 70°C for 15 minutes. The remaining albumin was analyzed by UV-Vis at 280 nm wavelength. The control solution was used without albumin, and the negative control experiment was conducted without the material. The decomposed inhibition was calculated by Equation (4):

$$\% \text{ inhibition} = \frac{OD_c - (OD_t - OD_{cs})}{OD_c} \times 100\% \quad (4)$$

where OD_c is the absorbance of the negative control, OD_t is the absorbance of the test sample, and OD_{cs} is the absorbance of the control solution.

2.6.3. Sapodilla preservation

Sapodilla was utilized to investigate the preservation of the film. Sapodilla were dip-coated in CTS-PVA-SeGO film solution and dried 4 times. The remaining weight was investigated to specify the film protection. Sapodilla were stored at room temperature for 6 days. Total soluble solids (^{o}Brix) was determined by a sugar-acid integrated machine (PLA-BXIACID1, ATAGO Ltd., Japan).

3. Results and discussion

3.1. Characteristics of SeMPs, GO, and SeGO

Figure 2 depicts the FTIR spectra of individual components of GO and SeMPs, while the SeGO composite was also analyzed to observe changes in the functional groups after anchoring SeMPs onto the surface of the GO sheets. It can be seen that three spectra of the GO, SeMPs, and SeGO composite exhibit two main regions of the signal at around 3700 – 3300 and 1700 – 1300 cm^{-1}. These oscillations respectively ascribe to the presence of the functional hydroxyl (–OH) groups, along with the occurrence of the –C=O stretching, which might have originated from the functionalities of hydroxyl, carboxyl, carbonyl, and ketone groups in both phyto-compounds and GO sheets.

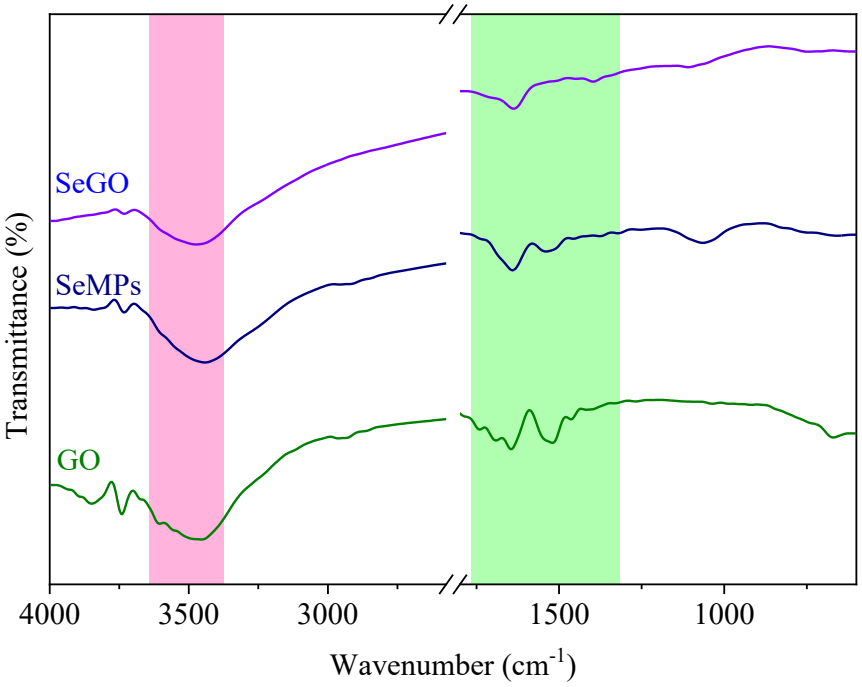


Figure 2. FTIR spectra of SeMPs, GO, and SeGO

The SEM images were performed to examine the morphology and microstructure of SeMPs, GO, and SeGO, as shown in Figure 3. It can be easily observed that the formation of SeMPs exhibits a nearly spherical shape and agglomerates into large clusters to reduce surface tension and enhance stability (Figure 3b). After anchoring SeMPs onto the GO network, the agglomeration of material was partially eliminated, as a result, the size of SeMPs is significantly reduced and evenly distributed on the GO network which is surrounded by functional groups present in the extract (Figure 3c) [15, 22].

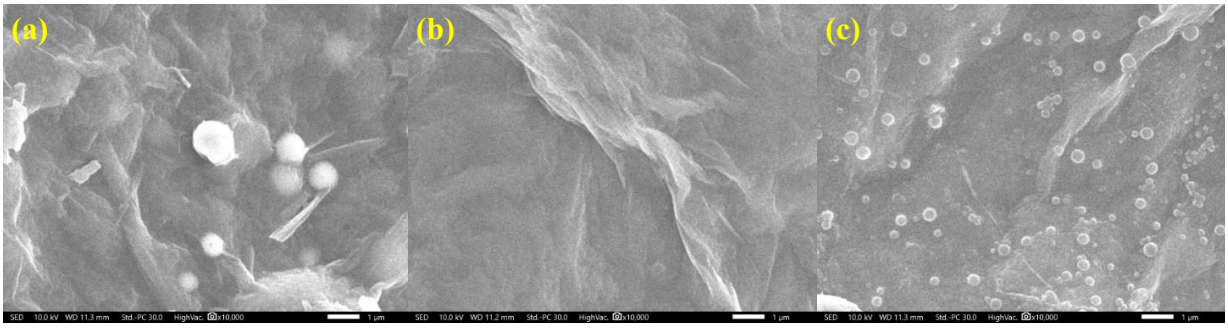


Figure 3. SEM images of (a) SeM`Ps, (b) GO, and (c) SeGO

Furthermore, the EDS spectrum and elemental mapping were analyzed to investigate the composition and distribution of elemental SeGO, as shown in Figure 4a and b. The EDS analysis

revealed two prominent peaks of Se at approximately 1.3 and 1.4 keV, indicating the successful doping of material onto the GO network. Additionally, the dominant presence of C and O was observed, which can originate from the carbon rid from GO and the reduction of certain phytochemicals in the extract. It is also clearly observed that the distribution of elements is uniform on the surface of the material, in which the main element S is contained on GO sheets owing to the usage of sulfuric acid in the GO procedure [23]. Accordingly, C and O account for almost the total amount (> 90% of the mass), while S and Se elements comprise less mass, about 2.41 and 6.05%, respectively. Hence, this confirms the successful synthesis and purification of SeGO without any impurities. This result is also consistent with previous studies.

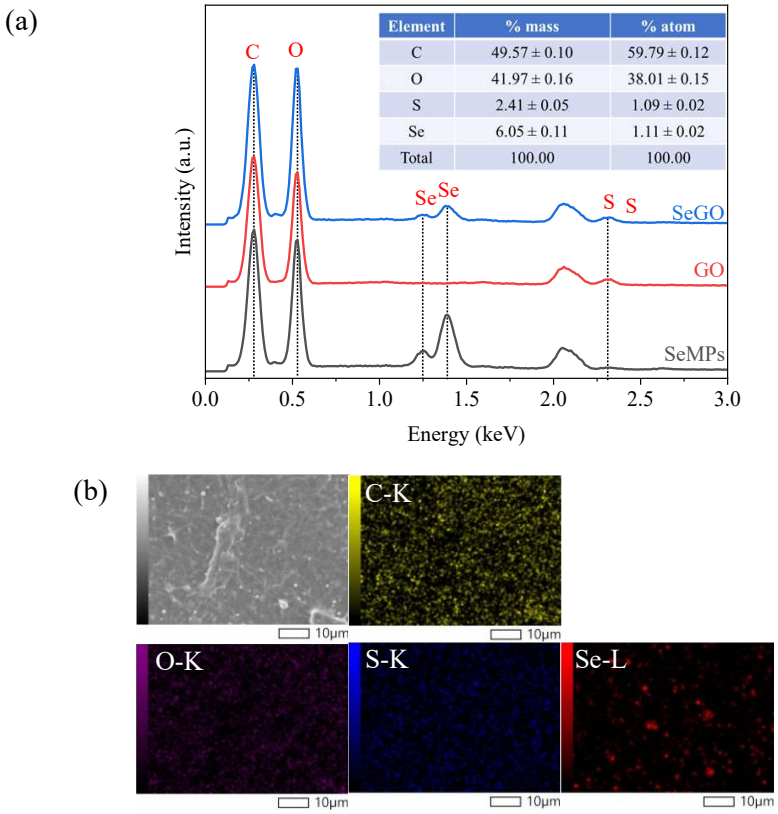


Figure 4. (a) EDS spectra of materials and (b) elemental mapping of SeGO

3.2. Simultaneously effects of CTS, PVA, and SeGO content on antibacterial activity of the film

The Box-Behnken design was used to assess the concurrent effects of different conditions, including the contents of CTS, PVA, and SeGO on the antibacterial performance of the prepared materials. According to Table 2, the inhibition percentage of the material ranged from 90 to 100%,

297 indicating the high antibacterial performance of all samples. Furthermore, the predicted results
298 obtained from the model also showed a similar trend when compared to the experimental values,
299 confirming the good reliability of the model. To be more specific, the analysis of variance
300 (ANOVA) was also derived from the model, as indicated in Table 3. Accordingly, the result
301 showed a high F-value (661.36) and low p-value (< 0.0001), revealing the statistical significance
302 of the model. The low p-values for C, P, S, CP, CS, PS, C^2, P^2, and S^2 also indicated the great
303 impacts of these variables on the response. Additionally, the correlation coefficient for the model
304 (R^2) was determined to be 0.99, compared to predicted and experimental predicted and adjusted
305 values, which also indicated the reliability of the model as well as the great adaptation between
306 the theoretical and experimental results. The coefficients of independent variables are given in
307 Equation (5). The equation shows that CTS, PVA, and SeGO contents influenced % inhibition in
308 a quadratic and linear model.

$$\% \text{ inhibition} = 72.2 + 9.975\ C - 0.275\ P + 19.225\ S - 1.9\ CP + 1.4\ CS - 0.775\ PS - 3.825\ C^2 - 0.31875\ P^2 - 3.175\ S^2 \quad (5)$$

309 **Table 2.** The central composite design presents the combination of coded and real values of
310 independent variables, the predicted and actual values of the response

Trials	Independent variables			% inhibition	
	CTS (g)	PVA (g)	SeGO (g)	Experimental	Predicted
1	2	4	2	99.8	99.80
2	1	2	2	100	100.17
3	1	6	2	90.1	90.27
4	1	4	3	95.5	95.35
5	2	4	2	99.8	99.80
6	3	4	1	92.9	93.05
7	2	2	1	94.3	94.32
8	2	6	1	95.1	95.12
9	2	2	3	98.7	98.67

10	2	4	2	99.8	99.80
11	2	4	2	99.8	99.80
12	3	4	3	91.3	91.50
13	2	6	3	93.3	93.27
14	3	6	2	97.0	96.82
15	3	2	2	91.7	91.52
16	1	4	1	91.5	91.30
17	2	4	2	99.8	99.80

311 **Table 3.** ANOVA analysis results

Source	Sum of Squares	df	Mean Square	F-value	p-value	
Model	212.58	9	23.62	661.36	< 0.0001	significant
C-CTS	2.20	1	2.20	61.74	0.0001	
P-PVA	10.58	1	10.58	296.24	< 0.0001	
S-SeGO	3.13	1	3.13	87.50	< 0.0001	
CP	57.76	1	57.76	1617.28	< 0.0001	
CS	7.84	1	7.84	219.52	< 0.0001	
PS	9.61	1	9.61	269.08	< 0.0001	
C^2	61.60	1	61.60	1724.87	< 0.0001	
P^2	6.84	1	6.84	191.65	< 0.0001	
S^2	42.44	1	42.44	1188.45	< 0.0001	
Residual	0.2500	7	0.0357			
Lack of Fit	0.2500	3	0.0833			
Pure Error	0.0000	4	0.0000			
Cor Total	212.83	16				

In Equation (5), the ideal ratio of CTS, PVA, and SeGO for the CTS-PVA-SeGO film comprises 1.95 g of CTS, 3.78 g of PVA, and 2.09 g of SeGO. At this film, the % inhibition reached 100%, falling within the 95% confidence interval of the predicted value (100%). These findings align with the ANOVA data as well (Table 4). So, the 2:4:2 ratio of CTS:PVA:SeGO (denoted as CPS) content was used for characterization, mechanical properties, and various applications in antibacterial activity, protein protection, and storage sapodilla.

Table 4. Antibacterial performance of the film

	Content (g)			% inhibition (%)	
	CTS	**PVA**	**SeGO**	**Experimental**	**Predicted**
Predicted	1.95	3.78	2.09	99.99	100.00
Corrected	2	4	2		

The simultaneous effects of different factors on the antibacterial activity of the material were also evaluated via the 3D response surface obtained from the model, as demonstrated in Figure 5. According to Figure 5a, the increase in the chitosan content from 1 to 1.5 g showed a considerable increase in the percentage of inhibition, indicating the enhanced antibacterial performance of the material. This tendency can be explained by the antibacterial effect of the chitosan, which induces a strong electrostatic interaction with the microorganisms, leading to the leakage of the intracellular contents of the bacteria. However, the further increase in the chitosan content showed a notable reduction in the inhibition percentage, which can be explained by the excessive content of the chitosan, which may increase the compactness of the film and inhibit the interaction between the SeGO and the bacteria. On the other hand, the figure for the PVA content also showed an analogous tendency. However, these parameters showed insignificant variation tendencies, which can be explained by the negligible antibacterial effect of the PVA [24]. However, it should be noted that the role of PVA is of paramount importance in the properties of the resulting material, contributing to the mechanical properties of the material. Moreover, the excessive addition of PVA may also attenuate the bioactivity by decreasing the biologically active surface due to the strong hydrogen bonding between the chitosan and the PVA molecules. Besides, the inhibition percentage of the prepared material also increased with the increase in the SeGO content, which re-affirms the promising antibacterial performance of the SeGO nanocomposites. However, the excessive increase in the SeGO content also led to a considerable decrease in the inhibition percentage, which

is ascribable to the aggregation of the Se particles during mixing, consequently leading to the reduction in the contact area with the bacteria.

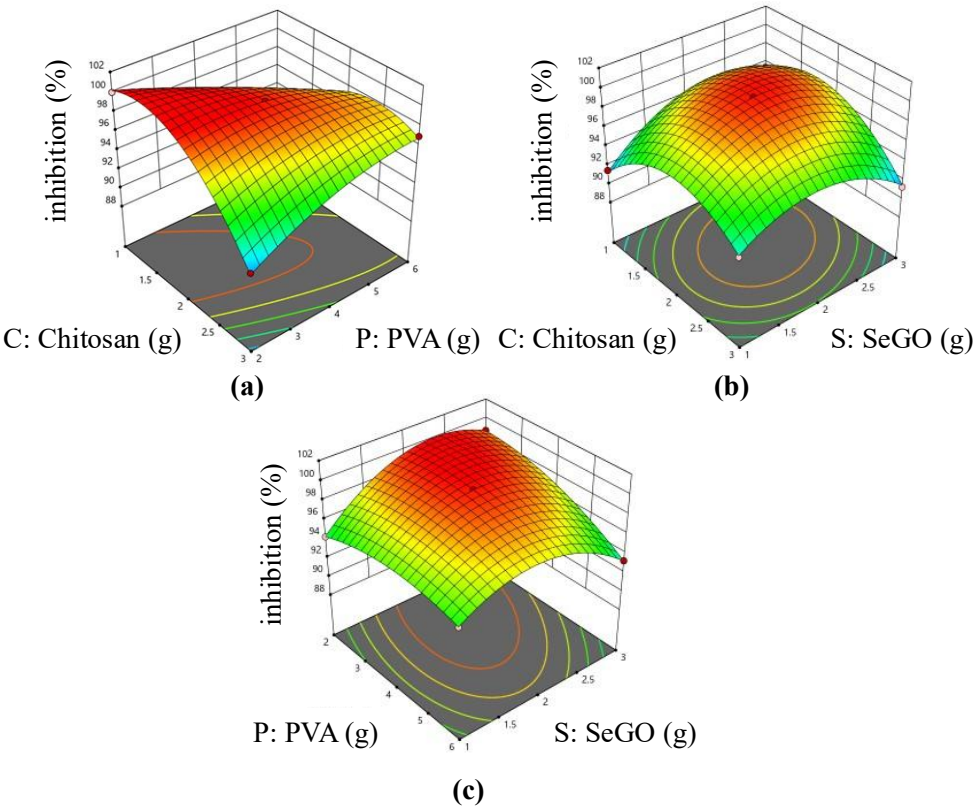


Figure 5. Response surface three-dimensional plots representing the interaction effect of each experimental variable on the response

3.3. Characteristics of films

The signal peaks appearing in pure materials mentioned in Figure 6 appear in the film with lower intensities. For further expectation, the appearance of the strong signal within the broad fluctuation of approximately 1150 cm^{-1}, corresponding to the existence of the C–N groups in CTS, can be observed in all samples that include the CTS component. However, the intensity of this peak fluctuates whenever there is presence or absence the PVA polymer in the matrix. Rather, the absorption bands at 1630 and 1420 cm^{-1} represented the functional bending signal of C=C vibrations and C–H bonds. Whereas, as compared to the pure materials, the samples containing the CTS indicate the slight shift and combination of two stretching oscillations of –OH and –NH persentation from alcohol and amine in the samples, respectively. Besides, the appearance of the medium C−H stretching is also recorded at nearly 2830 cm^{-1}, while this peak can no longer be in the case of pure materials. According to the result, there is an insignificant shift and decline in

intensity after the incorporation of three polymeric frameworks involving CTS, PVA, and SeGO, indicating the possibility of physical interaction for mechanical enhancement [18, 22 – 25].

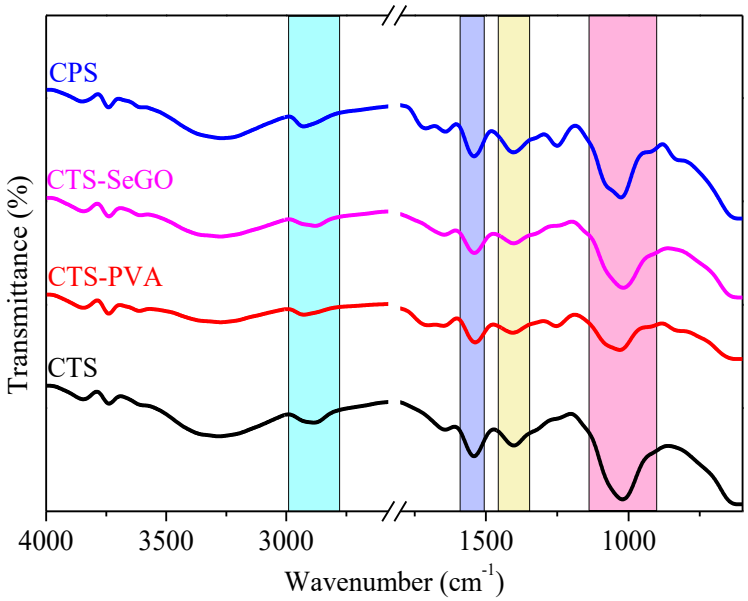


Figure 6. FT-IR Spectra of films

Figure 7 depicts the crystalline structure of the CTS-based samples with some points for attention. Outstandingly, the slight diffraction peaks at 2θ ~8.5, 11.3, and 15.3°, along with the strong occurrence of the signal at 2θ in a range of 18.2 – 22.7°. These figures are assigned to the semi-crystallization of the CTS, as can be seen in the XRD patterns of all samples. Notably, it can be observed that only pure CTS shows a strong peak at approximately 22.7°, while the addition of another polymer such as PVA makes the fluctuation conspicuously downward to 18.2°. Interestingly, with the presence of the PVA component, the obvious peak is frequently located at about 2θ ~19°, in contrast, the absence of this polymer indicates the most change in the location of this signal. Furthermore, the intensity of the strongest increases after loading the PVA into the CTS matrix, which might be explained by the appearance of the hydrogen bonding between them. The observation of the SeMPs is solely recorded and just exists only in the weak signal at about 2θ ~29.8°, corresponding to the (100) crystal plane. However, there is no longer existhe tence of signal of SeMPs when adding PVA into the matrix. This phenomenon can be explained by the increase of polymer matrix when combined PVA and CTS [22, 25]. It is affirmed that most of the as-prepared SeMPs form and possess the amorphous structure or another reason can be ascribed that the high intensity of the polymers overrides and suppresses the diffraction peaks of the SeNPs [15, 17].

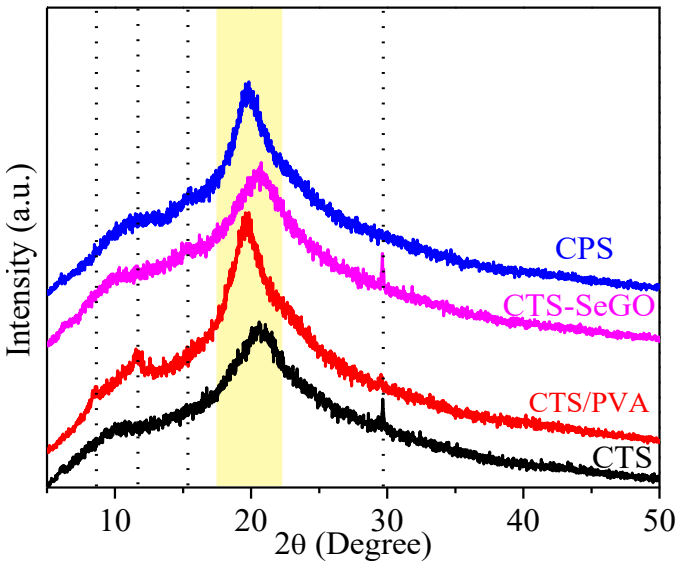


Figure 7. XRD patterns of films

The morphology and microstructure of the films were determined by SEM. In all four images of the synthesized films, the morphology of the film was continuous and uninterrupted due to the structure of two polymers, CTS and PVA. In Figure 8c, the white particles attached to the structure of the film can be easily observed. This indicates the successful attachment of SeGO to the structure of PVA. However, the structure of the film changed after PVA was added [15, 25]. This could be explained by the high water permeability and moisture of the CPS film, which altered the polymer structure of the film [26].

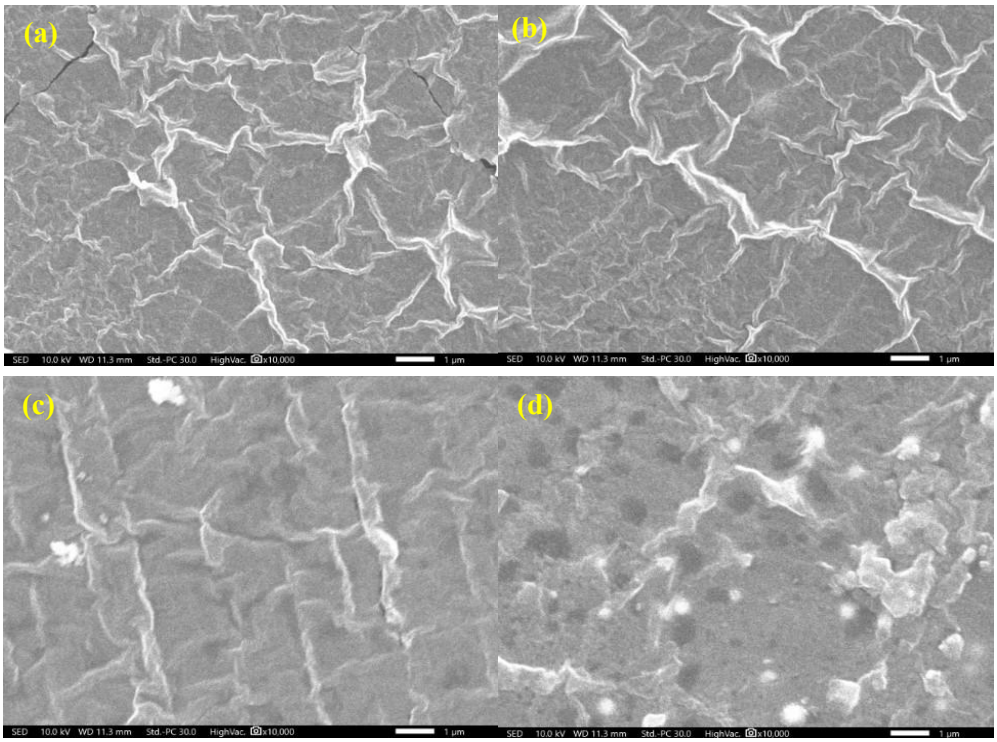
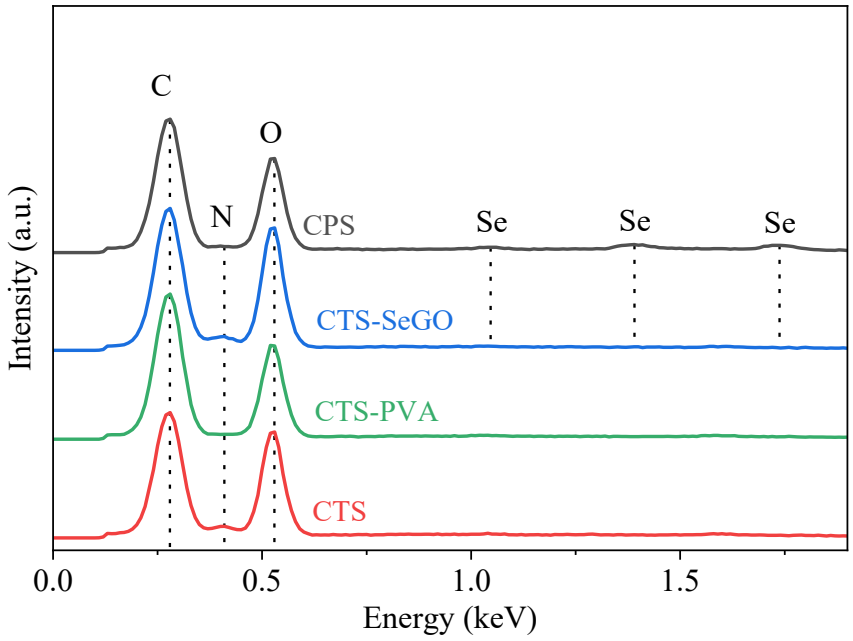


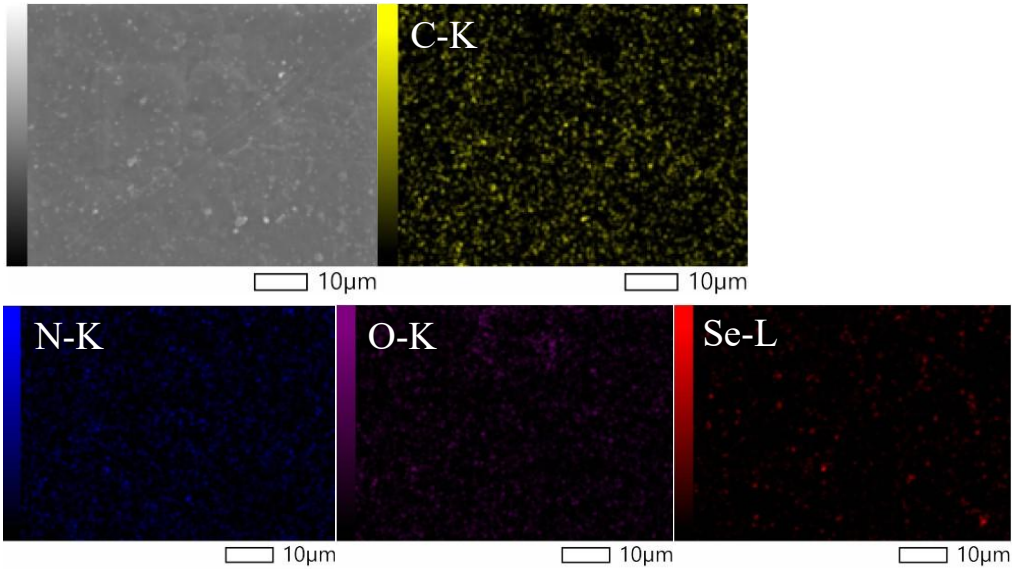
Figure 8. SEM images of (a) CTS, (b) CTS-SeGO, (c) CTS-PVA, and (d) CPS

The occurrence and distribution of elements in films were investigated using EDS and as shown in Figure 9. It was observed that the main elements involved in the films including C, O, N, and Se, were present. The EDS analysis revealed strong intensities of C and O at around 0.3 and 0.53 keV, respectively, indicating their origin from the carbon grid and the two polymer components present in the film. Additionally, the element Se was observed in the CTS-SeGO and CPS films at 1.2, 1.3, and 2.0 keV. This confirms the even dispersion of SeGO on the surface of the film. As results, it affirms the purity and absence of impurities in the film synthesis process. Figure 9c showed that the percentage of each element in the film. Selenium element accounts for only 3.22% mass in the CPS, while C and O occupies almost all of mass (54.84 and 41.92%, respectively). The ratio Se, C, and O mismatch with ratio of SeMPs in film, which may be attributed to SeMPs contain many phytocompound which play role in reduction and stabilition SeMPs.

(a)



(b)



(c)

Element	CTS	CTS-PVA	CTS-SeGO	CPS
C	48.97 ± 0.11	56.31 ± 0.12	48.25 ± 0.10	54.86 ± 0.12
N	3.59 ± 0.10	ND	3.91 ± 0.10	ND
O	47.44 ± 0.23	43.69 ± 0.22	47.68 ± 0.21	41.92 ± 0.21
Se	ND	ND	0.16 ± 0.07	3.22 ± 0.12

Figure 9. (a) EDS spectra, (b) elemental mapping, and (c) percent element of films

The thickness of the film and break energy were determined to evaluate the influence of SeGO and PVA on the mechanical properties of the film (Table 5). With the addition of PVA and SeGO to the film, the thickness increased sharply from 0.05 to 0.11 mm, and the break energy increased significantly from 2.15 to 59.29, respectively. This demonstrates that the incorporation of PVA and SeGO contributes to enhancing the quality of the film. Furthermore, the presence of SeGO can make the film denser due to the excellent dispersibility of SeGO on the surface of the film [26]. The improved dispersion of SeGO compared to PVA results in a better thickness of the film when combined with SeGO rather than PVA. The film made from mixing CTS and PVA exhibits high elongation (252.7%) but low mass load stress (19.01 MPa). By contrast, when combined with SeGO, the break elongation decreases significantly to nearly 13%, while the maximum load increases slightly by 1 MPa. This is attributed to the interaction between the –OH and $–NH_2$ groups of the two polymers, which enhances the mechanical strength of the film [27]. When all three components are combined, the percentage of break elongation increases significantly to 372.96%. This indicates that the addition of SeGO to CTS-PVA contributes to stabilizing the durability and improving the quality of the film.

Table 5. Mechanical properties of films

Mechanical properties*	Films			
	CTS	**CTS-PVA**	**CTS-SeGO**	**CPS**
Max load (N)	2.39 ± 0.75	10.99±0.84	9.87±24.00	10.43±1.78
Elasticity modulus (MPa)	1.37 ± 0.04	20.40 ± 1.37	2446.79 ± 807.62	26.20 ± 7.01
Max load stress (MPa)	4.77 ± 1.23	19.01 ± 1.53	5.77 ± 21.20	9.49 ± 1.62
Break elong (%)	74.35 ± 20.22	252.70 ± 42.75	12.99 ± 3.04	372.96 ± 17.95
Thickness (mm)	0.050 ± 0.008	0.058 ± 0.004	0.065 ± 0.024	0.110 ± 0.00
Break energy (kgf-mm)	2.15 ± 1.11	36.82 ± 8.28	11.28 ± 6.98	59.29 ± 13.43

*Values are described as Mean ± Standard Deviation (SD)

The swelling behavior of the film was assessed based on its structure and polymer composition. In food preservation, films need to exhibit good elasticity and durability in high-humidity environments, therefore, higher swelling value is undesirable. In Figure 10a, the pure CTS film showed the highest swelling among the three samples. However, after 6 hours, the water swelling decreased due to ~~the~~ interactions of H_2O and the $–NH_2$ groups in CTS. When combined with SeGO and PVA, the water swelling of the film was significantly reduced compared to the pure CTS film. This is because the materials coated on the entire surface of the film reduce its water affinity by substantially increasing the interaction and inhibiting the hydrophilic bonding with water molecules. Figure 10b shows the swelling behavior of the CTS-PVA film. After 100 minutes, the swelling of the film increased by 100%, but after this time the film tended to dissolve in water due to the hydrophilicity of PVA. The pure CTS film exhibited a high WVP due to the presence of hydrophilic groups in the structure of CTS. However, it still had a lower value compared to the film mixed with SeGO, which can be explained by the water-attracting nature of GO that increases the value of WVP. After the addition of PVA, the WVP decreased significantly. This can be attributed to the polymer coating on the surface of CTS and SeGO, which reduces the water vapor transmission rate of the film [28].

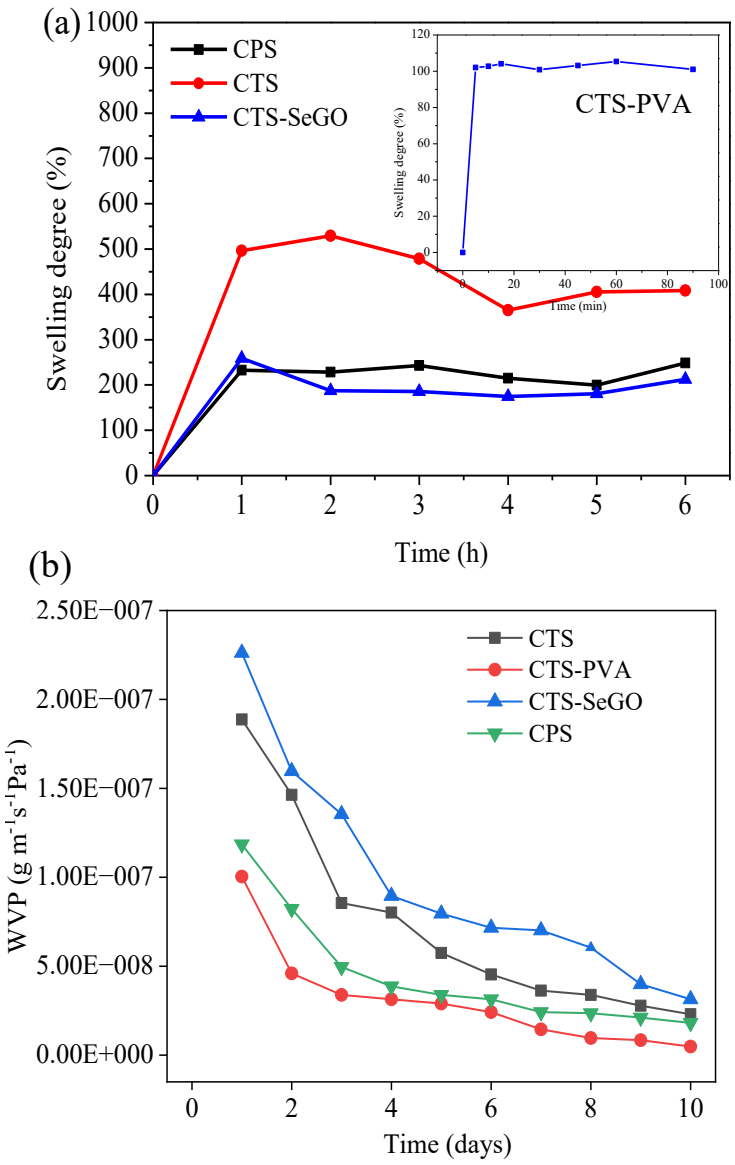


Figure 10. (a) Swelling degree (the inserted figure is the swelling result of the CTS-PVA film) and (b) water vapor permeability of CTS, CTS-PVA, CTS-SeGO, and CPS

3.4. Bioactivities of film

3.4.1. Antibacterial performance

For the applicability of the samples, the antibacterial activity of the film solution was assessed via the agar well diffusion method with results are depicted in Figure 11a. It is shown that the CTS-PVA-SeGO film exhibits greater antibacterial capacity than the three base films.

Additionally, enhanced antibacterial performance is observed against *E. coli* compared to *S. aureus*, which primarily attributed to variations in compositions and thickness of the bacterial cell walls [29]. The antibacterial ability of the film was improved when adding SeGO to the matrix.

As in previous studies, SeGO has good antibacterial ability against both Gram-negative and Gram-positive strains [9, 15, 22, 30]. Accordingly, in contact with bacterial cells, SeGO on the film directly impacts the bacterial cell wall by binding with functional groups on the surface and the sharp edges of the GO sheets. As reported, GO possesses a special structure within the superior amphiphilicity due to both hydrophilic functional groups on the surface and hydrophobic C-sheets. Hence, it results in the facilitation of the interaction between the materials and the cell film, breaking the semi-permeability of the film and facilitating the release of Se ions into the cytoplasmic cell. Furthermore, Se ions can interact with DNA (Deoxyribonucleic acid), proteins, and ribosomes, preventing the natural biosynthesis processes and disrupting structure, while the occurrence of DNA/protein denaturation is also exerted [31 – 33].

The antibacterial ability of the film is different between the *E. coli* strain and *S. aureus* strain. Figure 11b shows that, for the *S. aureus* strain, all the films had almost no resistance to this bacterial strain.

However, for *E. coli* strains, there is a clear inhibition zone. This is explained by the difference in cell wall structure of the nature of peptidoglycan between Gram-negative (*E. coli*) and Gram-positive (*S. aureus*) strains, as mentioned above. For Gram-positive bacteria, the cell wall is thicker and the cells also possess an outer capsule layer that prevents the interaction of materials with the cell. For Gram-negative strains, the cell wall is relatively thin and covered on the outside with a double layer of phospholipid film - a film with a structure that is both hydrophilic and hydrophobic - facilitating better contact of GO sheets with cell planning. Furthermore, the spherical-shaped cells of *S. aureus* also play an important role in resisting material contact compared to the rod-shaped cells of *E. coli*, this is due to the contact surface area between bacteria and material. On the other hand, the film solution samples give lower antibacterial capacity than individual SeMPs and GO samples. This is owing to the high viscosity of the film and the prevention originated from the presence of the polymer matrix, which limits diffusion inside the agar plate and, in turn, the antibacterial efficiency.

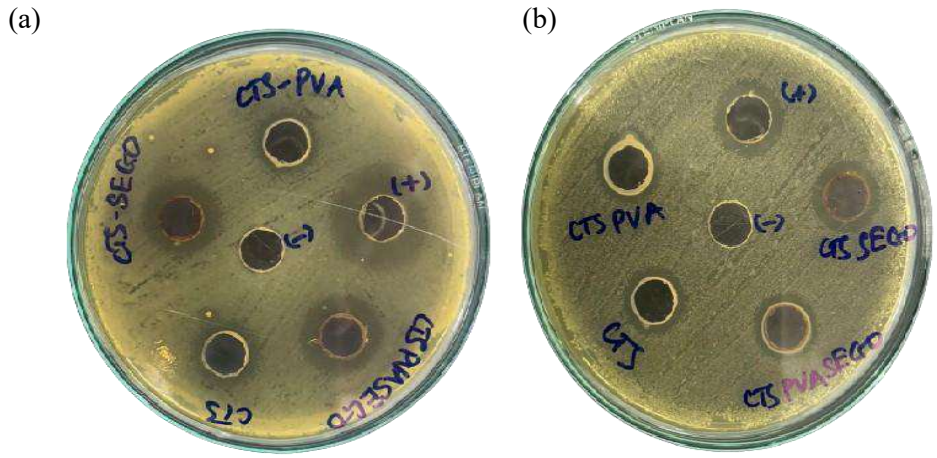


Figure 11. Antibacterial inhibition zones of CTS, CTS-PVA, CPS, and CTS-SeGO for (a) *E. coli* and (b) *S. aureus* film; (+) positive control: Gentamicin (10 µg/disc)

3.4.2. Anti-inflammatory activity

Albumin is a protein that contains biological functions. They contribute to the immune system by promoting the development of immune system receptors, which prevents antigen assault [34]. Non-steroidal anti-inflammatory medications (NSAIDs) have a stronger anti-inflammatory effect because the amount of albumin is not decreased. In this study, the anti-inflammatory activity of the film was investigated using egg albumin by determining the remaining contents after the shock-heating treatment. The findings revealed a consistent trend: as the concentration of film samples increased, their efficacy in inhibiting protein denaturation also increased. Interestingly, the CTS-PVA sample exhibited the lowest denaturation inhibition (~25%) at its maximum concentration, while other film samples demonstrated higher efficiency (~33%) at equivalent concentrations (Figure 12). This phenomenon may be caused by the coverage of PVA after adding it to the matrix, thereby reducing the inherent anti-inflammatory activity of CTS. This divergence suggests varying denaturation inhibition capabilities among the tested film compositions at their maximum concentration levels.

Studies on protein denaturation verify that the produced films have anti-inflammatory qualities in addition to improved food preservation [35]. The ability to inhibit heat-induced protein denaturation serves as a proof-of-concept for the film's active role in food preservation. By stabilizing proteins against thermal stress (70°C), the CPS film suggests a potential application in maintaining the nutritional integrity of protein-rich foods during storage and transport.

Preservation films can be used to package food and reduce protein loss, extending its shelf life relative to other foods. This is because they can withstand protein denaturation at high temperatures in traditional preservation film [36].

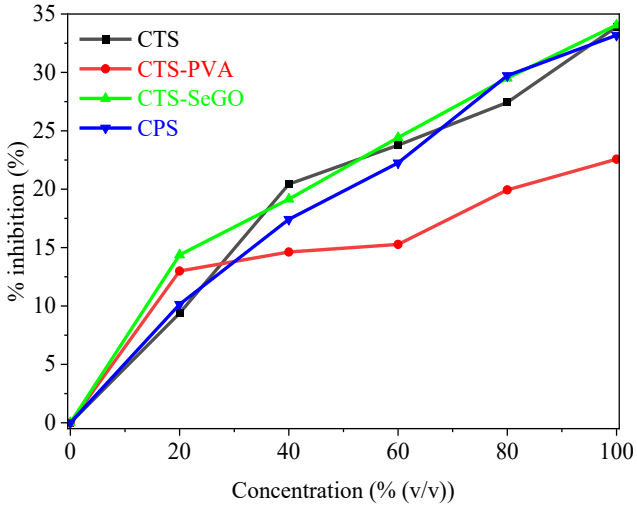


Figure 12. Anti-inflammatory of films

Other studies on selenium materials have also been listed in Table 6.

Table 6. Other studies on selenium materials**

Materials	Size (nm)	Antibacterial activity	References
rGO.SeNCs	180–250	MIC > 1000 µg/ml (*E. coli*) MIC > 200 µg/ml (*S. aureus*)	[37]
SeNPs	247	Inhubition zone of *P. aeruginosa* = 14.67 mm, *S. aureus* = 13.67 mm, and *E. coli* = 14.67 mm	[38]
ZnO@SeO	50	Inhibition zone of *S. aureus* = 28.33 mm, *B. subtilis* 27.33 mm, *B. cereus* = 27.67 mm , *P. aeruginosa* = 27.17 mm, *E. coli* = 27.5 mm, *S. typhi* = 24.33 mm against, *C. albicans* = 23.33 mm, and *A. niger* 18.17 mm.	[39]
CPS	270	Inhibiton zone of *E. coli* = 13 nm	In this study

** Abbreviation: rGO.SeNCs: graphene oxide encapsulated selenium nanoparticles; SeNPs: selenium nanoparticle; ZnO@SeO: zinc oxide nanoparticle-doped selenium oxide nanoparticles; MIC: mininum inhibitory concentration; *E. coli*: *Escherichia coli*; *S. aureus*: *Staphylococcus aureus*; *P. aeruginosa*: *Pseudomonas aeruginosa*; *B. subtilis*: *Bacillus subtilis; B. cereus*: *Bacillus cereus*; *S. typhi*: *Salmonella typhi*; *C. albicans*: *Candida albicans*, and *A.*

niger: *Aspergillus niger*.

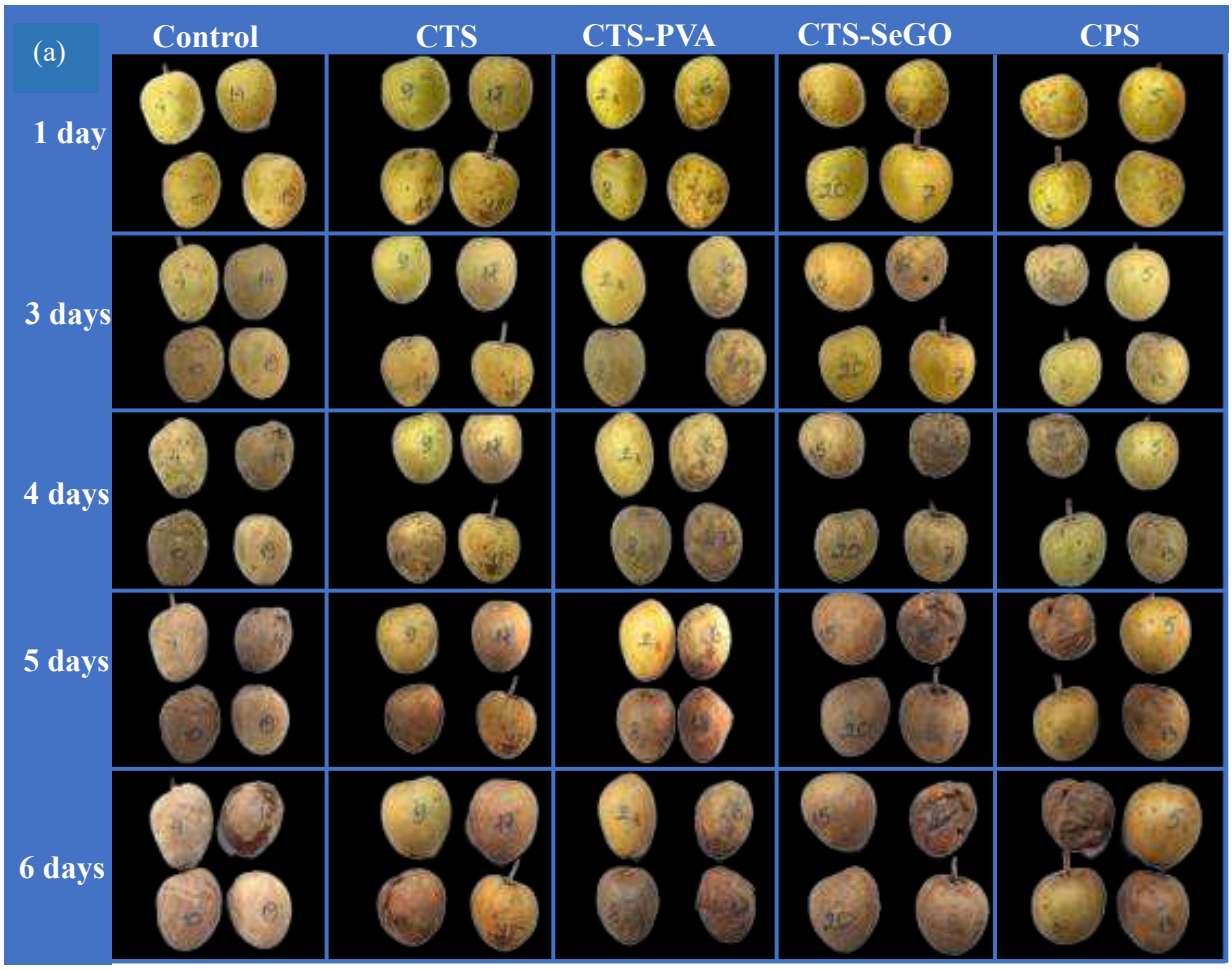
3.4.3. Sapodilla preservation

Following a 6-day survey, the sapodilla's size, shape, and color are displayed in Figure 14. As a result, after three days of storage, the weight of the sapodilla samples – both those with and without films – had significantly decreased, by more than 12.5% from the initial weight. After three days, the weight of the sapodilla with film decreased more than that of the sample without film.

Figure 13 demonstrates the capability of preserving sapodilla using the CPS film. After 6 days of preservation, the size and weight of the sapodilla decreased significantly, reaching only around 20% compared to the initial day in both samples, with and without the film. This weight loss can be attributed to the loss of moisture from the sapodilla. However, this weight loss is also one of the factors contributing to better preservation. The identified optimal ratio of 2:4:2 (CTS:PVA:SeGO) represents a critical physicochemical equilibrium for the composite film. In this ternary system, PVA acts as an essential plasticizer, mitigating the inherent brittleness of Chitosan through the formation of intermolecular hydrogen bonds, while SeGO provides the necessary mechanical reinforcement and bioactive sites. Deviations from this ratio resulted in diminished performance: excessive PVA content reduced the antimicrobial efficacy by burying the active SeGO sites, whereas a surplus of SeGO led to filler aggregation, compromising the film's structural continuity. Thus, the ratio 2:4:2 offers the precise balance required to maximize both the flexibility and the bioactive surface area of the packaging material. There was a notable presence of mold on the surface of the Sapodilla preserved without the CPS film. This phenomenon was absent in the samples preserved with the film (Figure 14). This difference is due to the mold-resistant property of SeGO, an element within the film that aids in better food preservation. With the film's ability to resist mold, the food preservation capability is enhanced, safeguarding the food from microbial agents, preventing their toxins, protecting consumers, and extending the preservation duration.

The resistance of film in preserving sapodilla against mold growth can be attributed to several mechanisms. Firstly, the films action induces water loss, reducing the overall moisture content of the sapodilla (as depicted in Figure 13b). This low moisture environment resembles the preservation method of drying sapodilla, effectively impeding the reproductive processes of the

sapodilla [40]. Secondly, the outer layer formed by CPS creates a barrier that obstructs the adhesion of mold to the sapodilla's surface [41]. This hinders the mold mycelium's ability to attach and proliferate, consequently impeding its reproductive cycle. Lastly, the SeGO material exhibits potent antifungal properties. Its presence on the film surface plays a significant role in penetrating and disrupting the structure of mold mycelium and spores, ultimately leading to the extermination of the mold. This action of SeGO contributes substantially to inhibiting mold growth on the preserved sapodilla [15, 22].



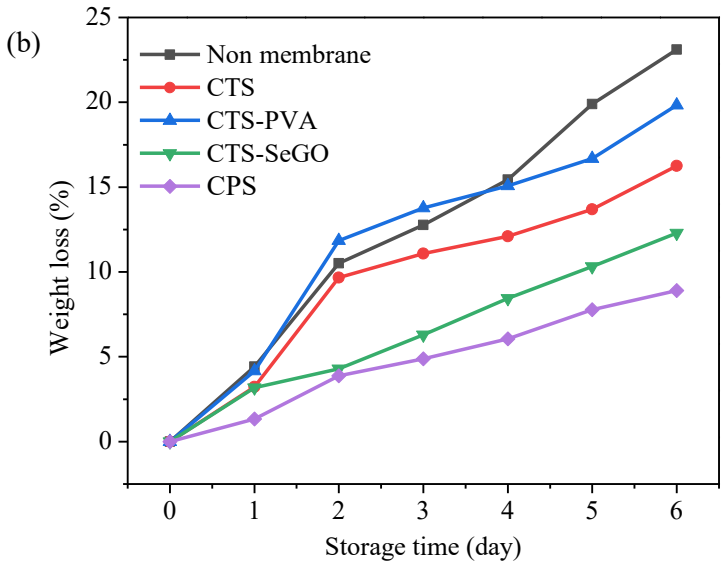


Figure 13. (a) The visual aspect of sapodilla without film, coated with CTS, CTS-PVA, CTS-SeGO, and CPS films and (b) the remaining weight of sapodilla after 6 days of storage at room temperature

From Figure 14, it can be seen that the soluble solids content of all sapodillas showed an initial trend of increasing and then gradually decreasing as the storage period lengthened. This is due to the hydrolysis of macromolecular polysaccharides into soluble sugars in citrus during the early stages of storage. During the later stages of storage, the reduced solids content is related to its participation in the respiratory process as a substrate. The control group showed the greatest change in soluble solids content, reaching a maximum value of 24% on day 3 and then decreasing rapidly. For coated sapodilla, the soluble solids content was more stable and the production and consumption of soluble solids was slower, suggesting that coatings may delay sapodilla ripening and inhibit respiration. Among them, the CPS group had the least variation in soluble solid content.

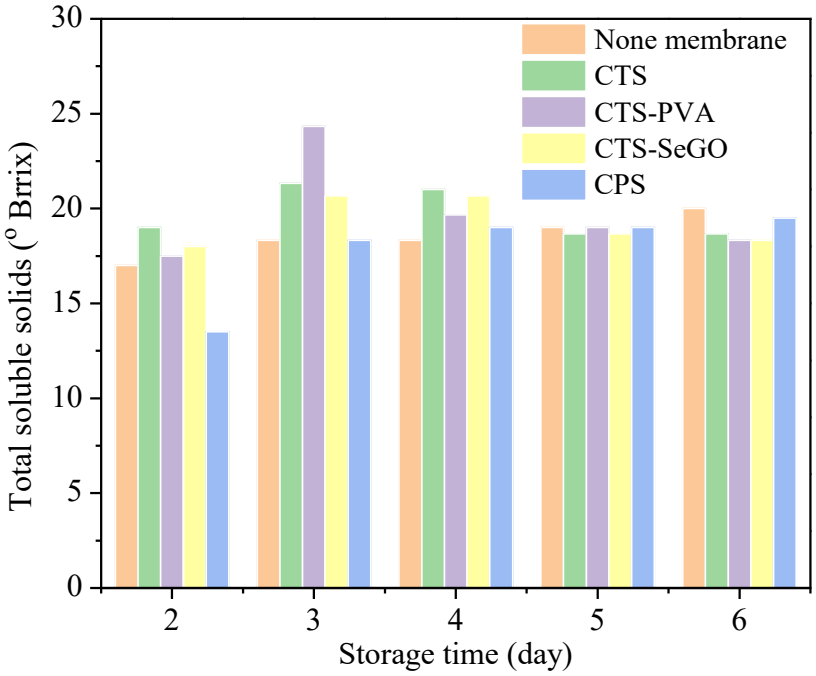


Figure 14. The concentration of total soluble solids in sapodilla without film, coated with CS, CTS-PVA, CTS-SeGO, and CPS during 6 days of storage at room temperature

4. Conclusion

In this study, SeGO composite was successfully prepared by using *P. guajava* leaf extract to synthesize SeMPs and sonication to decorate SeMPs onto the GO surface, while the fabrication of the chitosan-polyvinyl alcohol-selenium graphene oxide (CTS-PVA-SeGO) film was carried out *via* the casting method with the volume ratio between CTS, PVA, and SeGO at 2:4:2 (CPS) according to Box-Behnken model. In comparison with polymeric individuals or binary samples, the tripartite composite indicated an improvement in mechanical properties, swelling, water vapor permeability, and water solubility, which could be attributed to the role of the active packaging film for food preservation. Moreover, the CPS film also performed superior biological behaviors, comprising antibacterial activity and protein protection, which were evident in its application for sapodilla preservation. It was exerted that, with the encapsulation of the CPS film, the remaining weight of the sapodilla slightly decreased, the total soluble solid remarkably increased, and there was no appearance of the white mold outer the surface of the sapodilla during 6 days. These results affirm the reliable utilization of the film in food preservation, active packaging procedures, and sustainable development.

Acknowledgments

We acknowledge Ho Chi Minh City University of Technology (HCMUT), VNU-HCM for supporting this study.

Funding Declaration

The authors declare that no specific funding was received for this work.

Data availability statement

The datasets used and/or analysed during the current study are available from the corresponding author on reasonable request.

Author Contributions Statement

- Nguyen Ngoc Kim Tuyen, Nguyen Minh Dat: Investigation, Conceptualization, Methodology, Software, Writing - original draft
- Tran Do Dat: Investigation, Data curation, Writing – original draft
- Nguyen Huu Hieu: Project administration, Resources, Visualization, Writing- Reviewing and Editing.

Reference

[1] A. A. Alhwaige, T. Agag, H. Ishida, and S. Qutubuddin, "Biobased Chitosan/Polybenzoxazine Cross-Linked Films: Preparation in Aqueous Media and Synergistic Improvements in Thermal and Mechanical Properties," *Biomacromolecules*, vol. 14, no. 6, pp. 1806–1815, Jun. 2013, doi: 10.1021/bm4002014.

[2] F. J. Pavinatto, L. Caseli, and O. N. Oliveira, "Chitosan in Nanostructured Thin Films," *Biomacromolecules*, vol. 11, no. 8, pp. 1897–1908, Aug. 2010, doi: 10.1021/bm1004838.

[3] S. Khamhan, Y. Baimark, S. Chaichanadee, P. Phinyocheep, and S. Kittipoom, "Water Vapor Permeability and Mechanical Properties of Biodegradable Chitosan/Methoxy Poly(ethylene glycol)- *b* -Poly(ε-caprolactone) Nanocomposite Films," *International Journal of Polymer Analysis and Characterization*, vol. 13, no. 3, pp. 224–231, May 2008, doi: 10.1080/10236660802070652.

[4] M. Pereda, A. G. Ponce, N. E. Marcovich, R. A. Ruseckaite, and J. F. Martucci, "Chitosan-gelatin composites and bi-layer films with potential antimicrobial activity," *Food Hydrocoll*, vol. 25, no. 5, pp. 1372–1381, Jul. 2011, doi: 10.1016/j.foodhyd.2011.01.001.

[5] Y. Liu, S. Wang, W. Lan, and W. Qin, "Fabrication and Testing of PVA/Chitosan Bilayer Films for Strawberry Packaging," *Coatings*, vol. 7, no. 8, p. 109, Jul. 2017, doi: 10.3390/coatings7080109.

[6] M. Constantin *et al.*, "PVA/Chitosan Thin Films Containing Silver Nanoparticles and Ibuprofen for the Treatment of Periodontal Disease," *Polymers (Basel)*, vol. 15, no. 1, p. 4, Dec. 2022, doi: 10.3390/polym15010004.

[7] P. C. Srinivasa, M. N. Ramesh, K. R. Kumar, and R. N. Tharanathan, "Properties and sorption studies of chitosan–polyvinyl alcohol blend films," *Carbohydr Polym*, vol. 53, no. 4, pp. 431–438, Sep. 2003, doi: 10.1016/S0144-8617(03)00105-X.

[8] A. Svang-Ariyaskul *et al.*, "Blended chitosan and polyvinyl alcohol membranes for the pervaporation dehydration of isopropanol," *J Memb Sci*, vol. 280, no. 1–2, pp. 815–823, Sep. 2006, doi: 10.1016/j.memsci.2006.03.001.

[9] Y. Huang, E. Su, J. Ren, and X. Qu, "The recent biological applications of selenium-based nanomaterials," *Nano Today*, vol. 38, p. 101205, Jun. 2021, doi: 10.1016/j.nantod.2021.101205.

[10] Y. Fu, J. Wang, Q. Liu, and H. Zeng, "Water-dispersible magnetic nanoparticle–graphene oxide composites for selenium removal," *Carbon N Y*, vol. 77, pp. 710–721, Oct. 2014, doi: 10.1016/j.carbon.2014.05.076.

[11] Z. Lu, J. Yu, H. Zeng, and Q. Liu, "Polyamine-modified magnetic graphene oxide nanocomposite for enhanced selenium removal," *Sep Purif Technol*, vol. 183, pp. 249–257, Aug. 2017, doi: 10.1016/j.seppur.2017.04.010.

[12] C. Sainz-Urruela, S. Vera-López, M. P. San Andrés, and A. M. Díez-Pascual, "Graphene-Based Sensors for the Detection of Bioactive Compounds: A Review," *Int J Mol Sci*, vol. 22, no. 7, p. 3316, Mar. 2021, doi: 10.3390/ijms22073316.

[13] M. Constantin *et al.*, "PVA/Chitosan Thin Films Containing Silver Nanoparticles and Ibuprofen for the Treatment of Periodontal Disease," *Polymers (Basel)*, vol. 15, no. 1, p. 4, Dec. 2022, doi: 10.3390/polym15010004.

[14] S. Tripathi, G. K. Mehrotra, and P. K. Dutta, "Chitosan based antimicrobial films for food packaging applications," *e-Polymers*, vol. 8, no. 1, Dec. 2008, doi: 10.1515/epoly.2008.8.1.1082.

[15] N. N. K. Tuyen *et al.*, "Selenium microparticles decorated graphene oxide *via* green synthesis using *Psidium guajava* leaves: preparation, characterization, and biological activities," *New Journal of Chemistry*, vol. 47, no. 36, pp. 16993–17006, 2023, doi: 10.1039/D3NJ02443A.

[16] N. T. Huong *et al.*, "Optimization of the antibacterial activity of silver nanoparticles-decorated graphene oxide nanocomposites," *Synth Met*, vol. 268, p. 116492, Oct. 2020, doi: 10.1016/j.synthmet.2020.116492.

[17] I. Bano, M. Arshad, T. Yasin, and M. A. Ghauri, "Preparation, characterization and evaluation of glycerol plasticized chitosan/PVA blends for burn wounds," *Int J Biol Macromol*, vol. 124, pp. 155–162, Mar. 2019, doi: 10.1016/j.ijbiomac.2018.11.073.

[18] Q. T. Thanh Huong *et al.*, "Structurally natural chitosan films decorated with Andrographis paniculata extract and selenium nanoparticles: Properties and strawberry preservation," *Food Biosci*, vol. 53, p. 102647, Jun. 2023, doi: 10.1016/j.fbio.2023.102647.

[19] W. Wang, S. Han, Z. Jiao, J. Cheng, and J. Song, "Antioxidant Activity and Total Polyphenols Content of Camellia Oil Extracted by Optimized Supercritical Carbon Dioxide," *J Am Oil Chem Soc*, vol. 96, no. 11, pp. 1275–1289, Nov. 2019, doi: 10.1002/aocs.12285.

[20] T. T. Nguyen *et al.*, "Glycerol-plasticized chitosan film for the preservation of orange," *J Food Saf*, vol. 42, no. 1, Feb. 2022, doi: 10.1111/jfs.12943.

[21] A. Klančnik, S. Piskernik, B. Jeršek, and S. S. Možina, "Evaluation of diffusion and dilution methods to determine the antibacterial activity of plant extracts," *J Microbiol Methods*, vol. 81, no. 2, pp. 121–126, May 2010, doi: 10.1016/j.mimet.2010.02.004.

[22] N. T. H. Nam *et al.*, "Biological activity prospects of selenium-decorated graphene oxide composite by green synthesis using Sesbania sesban flower extract," *Diam Relat Mater*, vol. 141, p. 110563, Jan. 2024, doi: 10.1016/j.diamond.2023.110563.

[23] S. Zainab, M. Azeem, S. U. Awan, S. Rizwan, N. Iqbal, and J. Rashid, "Optimization of bandgap reduction in 2-dimensional GO nanosheets and nanocomposites of GO/iron-oxide for electronic device applications," *Sci Rep*, vol. 13, no. 1, p. 6954, Apr. 2023, doi: 10.1038/s41598-023-33200-4.

[24] E. Olewnik-Kruszkowska, M. Gierszewska, E. Jakubowska, I. Tarach, V. Sedlarik, and M. Pummerova, "Antibacterial Films Based on PVA and PVA–Chitosan Modified with Poly(Hexamethylene Guanidine)," *Polymers (Basel)*, vol. 11, no. 12, p. 2093, Dec. 2019, doi: 10.3390/polym11122093.

[25] N. M. Dat *et al.*, "Green synthesis of chitosan-based membrane modified with uniformly micro-sizing selenium particles decorated graphene oxide for antibacterial application," *Int J Biol Macromol*, vol. 220, pp. 348–359, Nov. 2022, doi: 10.1016/j.ijbiomac.2022.08.078.

[26] X. Yan *et al.*, "Characterization and bio-functional performance of chitosan/poly (vinyl alcohol)/trans-cinnamaldehyde ternary biopolymeric films," *Int J Biol Macromol*, vol. 246, p. 125680, Aug. 2023, doi: 10.1016/j.ijbiomac.2023.125680.

[27] M. N. Hyder and P. Chen, "Pervaporation dehydration of ethylene glycol with chitosan–poly(vinyl alcohol) blend membranes: Effect of CS–PVA blending ratios☆," *J Memb Sci*, vol. 340, no. 1–2, pp. 171–180, Sep. 2009, doi: 10.1016/j.memsci.2009.05.021.

[28] Z. Liu and X. Liu, “Enhanced Antibacterial Performance of Chitosan/Corn Starch Films Containing TiO2/Graphene for Food Packaging,” *Polymers (Basel)*, vol. 14, no. 18, p. 3844, Sep. 2022, doi: 10.3390/polym14183844.

[29] J. Zhang, P. Su, H. Chen, M. Qiao, B. Yang, and X. Zhao, “Impact of reactive oxygen species on cell activity and structural integrity of Gram-positive and Gram-negative bacteria in electrochemical disinfection system,” *Chemical Engineering Journal*, vol. 451, p. 138879, Jan. 2023, doi: 10.1016/j.cej.2022.138879.

[30] I. Riyal *et al.*, “Antimicrobial activity of synthesized graphene oxide-selenium nanocomposites: A mechanistic insight,” *Environmental Science and Pollution Research*, vol. 30, no. 7, pp. 19269–19277, Oct. 2022, doi: 10.1007/s11356-022-23550-3.

[31] H. Zheng *et al.*, “Antibacterial applications of graphene oxides: structure-activity relationships, molecular initiating events and biosafety,” *Sci Bull (Beijing)*, vol. 63, no. 2, pp. 133–142, Jan. 2018, doi: 10.1016/j.scib.2017.12.012.

[32] S. Bhatt, V. D. Punetha, R. Pathak, and M. Punetha, “Graphene in nanomedicine: A review on nano-bio factors and antibacterial activity,” *Colloids Surf B Biointerfaces*, vol. 226, p. 113323, Jun. 2023, doi: 10.1016/j.colsurfb.2023.113323.

[33] S. Bhatt, V. D. Punetha, R. Pathak, and M. Punetha, “Graphene in nanomedicine: A review on nano-bio factors and antibacterial activity,” *Colloids Surf B Biointerfaces*, vol. 226, p. 113323, Jun. 2023, doi: 10.1016/j.colsurfb.2023.113323.

[34] V. Arroyo, R. García-Martinez, and X. Salvatella, “Human serum albumin, systemic inflammation, and cirrhosis,” *J Hepatol*, vol. 61, no. 2, pp. 396–407, Aug. 2014, doi: 10.1016/j.jhep.2014.04.012.

[35] R. B. Bodini, S. M. P. Pugine, M. P. de Melo, and R. A. de Carvalho, “Antioxidant and anti-inflammatory properties of orally disintegrating films based on starch and hydroxypropyl methylcellulose incorporated with Cordia verbenacea (erva baleeira) extract,” *Int J Biol Macromol*, vol. 159, pp. 714–724, Sep. 2020, doi: 10.1016/j.ijbiomac.2020.05.075.

[36] S. Xu, X. Chen, and D.-W. Sun, “Preservation of kiwifruit coated with an edible film at ambient temperature,” *J Food Eng*, vol. 50, no. 4, pp. 211–216, Dec. 2001, doi: 10.1016/S0260-8774(01)00022-X.

[37] S. Naemi and A. Meshkini, “Phytosynthesis of graphene oxide encapsulated selenium nanoparticles using Crocus Sativus petals’ extract and evaluation of their bioactivity,” *J Drug Deliv Sci Technol*, vol. 81, p. 104286, Mar. 2023, doi: 10.1016/j.jddst.2023.104286.

[38] N. N. K. Tuyen *et al.*, "Applicable orientation of eco-friendly phyto-synthesized selenium nanoparticles: Bioactive investigation and dye photodegradation," *Biomass Convers Biorefin*, Jan. 2023, doi: 10.1007/s13399-023-03823-8.

[39] H. Qanash *et al.*, "Bioenvironmental applications of myco-created bioactive zinc oxide nanoparticle-doped selenium oxide nanoparticles," *Biomass Convers Biorefin*, Feb. 2023, doi: 10.1007/s13399-023-03809-6.

[40] D. Dhanapal and B. Rajoo, "Value addition of mushrooms by incorporation in the food products: an overview," *International Journal of Food Engineering*, vol. 19, no. 12, pp. 573–591, Dec. 2023, doi: 10.1515/ijfe-2023-0073.

[41] Y. Habibi and L. A. Lucia, Eds., *Polysaccharide Building Blocks*. Wiley, 2012. doi: 10.1002/9781118229484.

Graphical Abstract

